COMMUNICATION

N-type Rigid Semiconducting Polymers Bearing Oligo(Ethylene Glycol) Side Chains for High Performance Organic Electrochemical Transistors

Xingxing Chen,*[a] Adam Marks,[b] Bryan D. Paulsen,[c] Ruiheng Wu,[d] Reem B. Rashid,[c] Hu Chen,[a] Maryam Alsufyani,[a] Jonathan Rivnay,[c][e] and Iain McCulloch*[a][b][f]

[a] M. Alsufyani, Dr. X. Chen, H. Chen, Prof. I. McCulloch
Department of Physical Science and Engineering Division
King Abdullah University of Science and Technology (KAUST)
Thuwal, 23955-6900, Saudi Arabia.
E-mail: xingxing.chen@kaust.edu.sa, iain.mcculloch@chem.ox.ac.uk

[b] Dr. A. Marks, Prof. I. McCulloch
Department of Chemistry and Centre for Plastic Electronics
Imperial College London
London, W12 0BZ, UK.

[c] Dr. B. D. Paulsen, R. B. Rashid, Prof. J. Rivnay
Department of Biomedical Engineering
Northwestern University
2145 Sheridan Rd, Evanston, IL 60208, USA.

[d] R. Wu
Department of Chemistry
Northwestern University
2145 Sheridan Rd, Evanston, IL 60208, USA.

[e] Prof. J. Rivnay
Simpson Querrey Institute
Northwestern University
Chicago, Illinois 60611, USA.

[f] Prof. I. McCulloch
Department of Chemistry, Chemistry Research Laboratory
University of Oxford
Oxford, OX1 3TA, UK.

Supporting information for this article is given via a link at the end of the document.

Abstract: N-type conjugated polymers as the semiconducting component of organic electrochemical transistors (OECTs) are still undeveloped with respect to the p-type counterparts. Herein, we first report two rigid n-type conjugated polymers bearing oligo(ethylene glycol) (OEG) side chains, PgNaN and PgNgN, which demonstrated an essentially torsion-free π-conjugated backbone. The planarity and electron-deficient rigid structures enable the resulting polymers to achieve high electron mobility in an OECT device of up to 10^{-3} cm² V^{-1} s^{-1} range, with a deep-lying lowest unoccupied molecular orbital (LUMO) energy level lower than -4.0 eV. Prominently, the polymers exhibited a high device performance with a maximum dimensionally normalized transconductance of 0.212 S cm^{-1} and the product of charge carrier mobility μ and volumetric capacitance C* of 0.662 ± 0.113 F cm^{-1} V^{-1} s^{-1}, which are among the highest in n-type conjugated polymers reported to date. Moreover, the polymers are synthesized via a metal-free aldol condensation polymerization, which is beneficial to their application in bioelectronics. Our work proves a new way for designing glycolated n-type conjugated polymers with low-lying LUMO and conformation-locked backbones for high performance OECTs.

Organic electrochemical transistors (OECTs) have attracted great attention in recent years as a promising device used for organic bioelectronics due to their low operation voltages, high sensitivity, good biocompatibility, operability in aqueous environments, as well as excellent signal amplification characteristics.[1] The core component of an OECT is a mixed conducting conjugated polymer which is able to efficiently conduct both electronic and ionic charge carriers. The electroactive polymers constituting the channel of OECT are in direct contact with an electrolyte and with the source and drain metal electrodes. As a result, ions are able to penetrate from electrolyte into the bulk of the transistor channel while a gate voltage (V_G) is applied in an OECT device. Subsequently, the ionic signals can be transduced into electronic ones.[2] The transduction efficiency is quantified in the OECT transconductance ($g_m = \partial I_d/\partial V_g$), which is one of the most important figures of merit for an OECT device and is affected by the properties of the channel polymers, such as, carrier mobility and ion transportation.[3] Thus, in-depth understanding the structure−property relationship of the semiconducting polymers is crucial to design new high-performance materials for OECT applications. Several ways to improve the mobility of conjugated polymers have been demonstrated in polymer solar cells (PSCs) and organic field-effect transistors (OFETs): enhancing backbone planarity, increasing the crystallinity of conjugated polymers, modifying the molecular weight, etc.[4] On the contrary, a closely packed and crystalline polymer has been shown to give rise to adverse ionic transportation. To strike the best compromise between electron mobility and ion penetration in conjugated polymers, side chain modification is an efficient way to enhance ion uptake while maintain a high mobility within the arrangement of polymer backbones.[5] Conjugated polymers with hydrophilic or ion-transporting side chains have been developed for OECTs with high transconductance to mS range, for example,

poly(2-(3,3'-bis(2-(2-(2-methoxyethoxy)ethoxy)ethoxy)-[2,2-bithiophen]-5-yl)thieno[3,2-b]thiophene) (Pg2T-TT), poly(2,5-diyl-3,4-[2,2-di(2,5,8,11-tetraoxadodecyl)propylene]-dioxythiophene-*alt*-2',5'-diyl-3',4'-[2,2-dimethylpropylene]-dioxythiophene) (ProDOT(OE)-DMP) and poly(3,4-ethylenedioxythiophene)sulfonate (PEDOT-S).[6] However, the vast majority of active polymers reported for OECTs so far are p-type materials, while n-type counterparts are lag far behind both in performance and availability[7].

N-type conjugated polymers have been extensively developed and investigated in OFETs and PSCs over the past decades, but less so for electrochemical transistors, mainly due to their low performance, and the lack of robust design rules to achieve high mixed mobility and stability in aqueous conditions. The majority of current n-type semiconducting polymers are donor(D)-acceptor(A) alternating co-polymers, synthesized via a transition metal-mediated cross coupling polymerization. The alternation of electron-rich and electron-deficient units of the polymers is facilitated with single bonds along the backbone, and promotes molecular orbital hybridization.[8] Rationally, rotational torsions around these single bonds are allowed which will give rise to conformational disorder, and consequently lead to a negative effect on the charge carrier mobility of the polymers. Meanwhile, the highly localized distribution of the LUMO frontier orbitals of D-A polymers further hinders intermolecular charge hopping and subsequently the charge carrier mobility.[9] Typically, the electron withdrawing functionality along these polymers is either insufficiently strong or prevalent to ensure that the polymer has a high enough electron affinity (EA) required to both facilitate electron injection, reduce the influence of shallow trapping and ensure the oxidative stability of the n-doped polymers, in operation in the presence of oxygen and/or in aqueous environment.[10] In addition, residual metallic species arising from polymerization, such as organostannannes as well as the transition metal catalysts, present a limitation for the polymers to be applied in bioelectronics. Thus, it is desirable to design polymers that comprise only of electron-deficient repeat units into the polymer backbone, have a delocalized LUMO energy level distribution, and eliminate torsional twists along the backbone. A series of conjugated n-type polymers with oligo(ethylene glycol) (OEG) side chains, are herein reported, with low-lying LUMO energy levels, polymerized via a metal-free aldol condensation, where all the repeat units are electron-deficient and locked in-plane by double bond linkers for use in electrochemical transistors.

OEG chains have been previously used in semiconducting polymer side chains for OECT applications[3b, 5b, 6a, 11] owing to their hydrophilicity and solubility. It has been demonstrated that replacing alkyl chains by glycol analogues endow the resulting semiconducting polymers with a decreased π-π stacking distance,[12] higher dielectric constant,[12a, 13] larger volumetric capacitance and higher ion uptake.[1h, 11c, 14] It has also been reported oxygen atoms along OEG chains can coordinate with the ions facilitating penetration into the polymer morphology from the electrolyte, in a manner similar to crown ethers, and enhance ion transport.[15] Herein, we report novel n-type semiconducting polymers that simultaneously incorporate a rigid π-conjugated backbone and OEG side chains. Owing to the high rigidity and planarity of the polymer backbone and the lack of donor-acceptor character, the LUMO frontier orbitals are highly delocalized which leads to a high electron mobility of 10^{-3} cm² V^{-1} s^{-1} range, measured in an OECT. Meanwhile, both polymers exhibited a deep-lying LUMO energy level lower than -4.0 eV due to an all electron-deficient polymer backbone. While applied in OECTs, the polymers demonstrated a high device performance with a maximum dimensionally normalized transconductance reaching 0.212 S cm^{-1} and the product of charge carrier mobility μ and volumetric C* (μC^*) of 0.662 ± 0.113 F cm^{-1} V^{-1} s^{-1}, which are higher than previously reported glycolated polymers, and comparable with the best performing BBL polymer.[11c, 16] Additionally, as prepared through a metal-free aldol condensation polymerization, these polymers should have a low concentration of toxic residues and be good candidates for bioelectronics. To the best of our knowledge, these are the first reported rigid n-type conjugated polymers with OEG side chains for OECT applications.

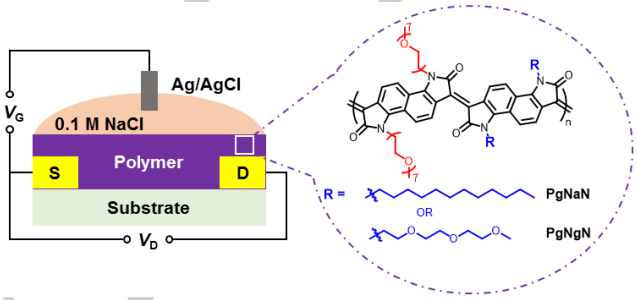

Figure 1. The typical structure of an OECT device (left) and the chemical structures (right) of PgNaN and PgNgN.

The chemical structures of the polymers, PgNaN and PgNgN, are shown in Figure 1. Both polymers comprise of fused electron-deficient lactam rings with OEG (and also alkyl in the case of PgNaN) side chains. To investigate the effect of OEG side chains on ion transport, the two polymers were designed to have a differing ratio of OEG groups, with PgNgN having a higher OEG chain density than that of PgNaN. As shown in Figure S1, the bis-isatin monomer was synthesized by a substitution reaction with bis-isatin and the iodine end-capped glycol chain. The most challenging step is to carry out the purification processes of glycolated bis-isatin monomer due to its large polarity and sticky physical nature. Finally, the pure monomer was obtained through recycling gel permeation chromatography (GPC) following earlier purification procedures of precipitation and silica gel column chromatography. Both polymers were prepared via acid-catalyzed aldol polymerization in toluene, which is more sustainable and benign to the environment compared with transition-metal-catalyzed polymerizations.

Table 1. Molecular weight, photophysical and energy level properties of PgNaN and PgNgN.

	M_n/M_w (kg/mol)	PDI	IP[a] (eV)	EA[b] (eV)	EA[c] (eV)	λ^{peak} (film/sol.)[d] (nm)	E_g^{opt},[e] (eV)
PgNaN	20.7/162.1	7.8	5.14	4.09	4.28	916/912	1.05
PgNgN	8.7/19.3	2.2	5.22	4.16	4.35	896/893	1.06

[a] Measured by photoelectron spectroscopy in air (PESA). [b] Calculated from E_g^{opt} and IP. [c] Calculated from the onset of electrochemical reduction. [d] The lower energy absorption peak of thin film and solution. [e] Estimated optical gap calculated using onset of film absorption spectra ($E_g^{opt} = 1240/\lambda_{onset}$).

It was observed that as the density of OEG chains get higher, the solubility of the resulting polymers significantly reduces during

polymerization and the reaction solution becomes a gel at room temperature. This contributes to the lower molecular weight of PgNgN compared to PgNaN (Table 1). The high PDI of PgNaN measured by GPC may be ascribed to its strong aggregation behavior resulting from the rigid polymer backbone. Both PgNaN and PgNgN show good solubility only in chloroform, with limited solubility in other common solvents, for example, chlorobenzene (CB), *o*-dichlorobenzene (*o*-DCB), 1,1,2,2-tetrachloroethane and dimethylformamide (DMF). Thermogravimetric analysis (TGA) measurements indicate that both PgNaN and PgNgN exhibit good thermal stability with thermal degradation temperature (T_d) higher than 330 °C (Figure S10).

The UV-Vis NIR absorption spectra of PgNaN and PgNgN in thin film and solution are shown in Figure S12. Both polymers exhibit broad absorption up to 1200 nm with a narrow band gap of 1.05 eV for PgNaN and 1.06 eV for PgNgN (listed in Table 1). There are two significant absorption peaks of the polymers, a higher-energy band in the visible and a broad NIR absorption band. It was demonstrated previously[10c] by time dependent density functional theory (TD-DFT) and solvatochromic experiments that the NIR absorption bands are not as a result of intermolecular charge transfer, and thus have little donor acceptor character. Ionization potentials (IP) of the two polymers were estimated by photo-electron spectrometer in air (PESA) and the electron affinity (EA) were calculated by subtracting the optical band gap from the IP values, the results are summarized in Table 1. Both PgNaN and PgNgN show a high EA up to 4.09 eV and 4.16 eV, respectively, which can facilitate electron injection and potential stability of the polymers in aqueous environment. The EA of both polymers were also estimated by cyclic voltammetry (Table 1 and Figure S13). The electrochemically derived EA levels are larger but share the same relative trends. The high EA of the two polymers may benefit from their all electron-deficient conjugated backbone.

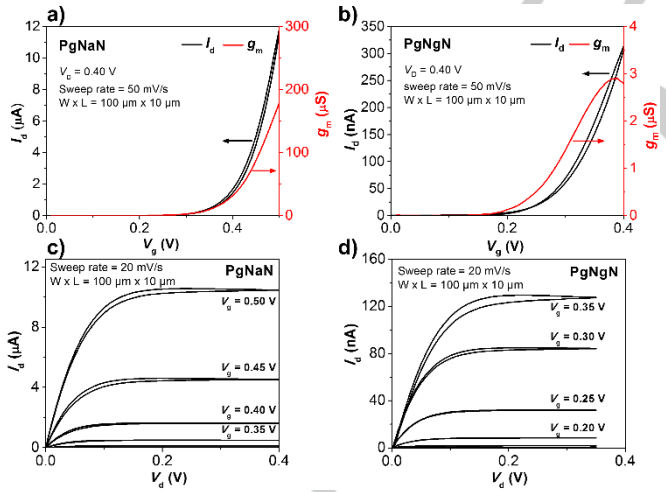

Figure 2. Organic Electrochemical Transistors: Transfer curves and voltage dependent transconductance of (a) PgNaN and (b) PgNgN. Output curves of (c) PgNaN and (d) PgNgN.

To evaluate the electrical properties of PgNaN and PgNgN, OECTs employing these two polymers as the channel material were fabricated with gold electrodes (source and drain) patterned on a glass substrate, illustrated in Figure 1. The conjugated polymer was deposited by drop casting without additives or further annealing steps, and the device was operated in an aqueous 0.1 M NaCl solution with an Ag/AgCl gate electrode. To provide a better comparison between the two polymers in this work and previously reported polymers, the maximum transconductance ($g_{m,max}$) values have been normalized by the channel geometry: $g_{m,max,norm.} = g_{m,max}/(Wd/L)$, where W is the channel width (100 µm), L is the channel length (10 µm), and d is the thickness of the electroactive layer (1500 nm for PgNaN and 500 nm for PgNgN), respectively.

The transfer and output characteristics of PgNaN and PgNgN based OECTs are shown in Figure 2 and summarized in Table 2. PgNaN based OECTs displayed ideal saturation behavior (squared increase in I_d and linear increase in g_m) out to V_g of 0.5 V. The maximum g_m value (0.212 S cm^{-1}) of PgNaN based OECT was reached at V_g of 0.58 V. The threshold voltage (V_t) of PgNaN based devices was extrapolated to be 0.37 ± 0.01 V. In comparison, PgNgN based OECT threshold voltage was 160 mV lower (V_t = 0.21 ± 0.02 V), reflecting the similar trend in EA. PgNgN OECTs displayed much lower drain currents, and a g_m peak around 0.007 S cm^{-1} at V_g of 0.38 V. When measuring transfer curves on PgNgN based device beyond V_g = 0.4 V, the maximum I_d reached showed large drops with each successive transfer curve, indicating electrochemical degradation of the PgNgN channel. The saturation mobilities of PgNaN and PgNgN were calculated to be 6.5 × 10^{-3} and 1.9 × 10^{-4} cm^2 V^{-1} s^{-1}, respectively. The rigid π-backbones with only electron-deficient repeat units help facilitate delocalized LUMO frontier orbitals and strong interchain interactions, enhancing the intra- and interchain carrier transport. The significantly poorer performance of the PgNgN polymer is likely to arise from its low molecular weight, which in turn arises from poor solubility during polymerization. The volumetric capacitance (C*) measured by electrochemical impedance spectroscopy (EIS) (Figure S14) for PgNgN was 239 F cm^{-3} while for PgNaN was 103 F cm^{-3}, presumed to arise from the 50% hydrophobic alkyl side chain.

A common figure of merit for OECT is μC*, which quantifies the intrinsic source of transconductance of a channel material. The μC* of PgNgN (0.037 ± 0.016 F cm^{-1} V^{-1} s^{-1}) is similar to state of the art glycolated N-type polymer OECT channel materials.[5b] Interestingly, however, the μC* of PgNaN (0.662 ± 0.113 F cm^{-1} V^{-1} s^{-1}) is much higher. Increasing V_g to 0.6 V revealed a g_m peak for PgNaN (0.212 S cm^{-1}) (Figure S15a), where the device no longer followed ideal saturation behavior. This has been variously attributed to contact resistance, DOS/disorder, and non-linear dopant/carrier density across the length of the OECT channel.[17] Beyond 0.6 V electrochemical degradation was significant as I_d decreased sweep-to-sweep. The stability of PgNaN OECTs up to V_g = 0.6 V was established by continuous ON-OFF cycles via repeated gate pulsing, as shown in Figure S15e. On currents displayed an initial “break in”, stabilizing at 75% of that of the first measurement. PgNaN seems to exhibit an optimal balance of hydrophilic/hydrophobic behaviour, providing a hydrated channel for ionic diffusion without overly swelling, thus retaining structural order.

Spectroelectrochemistry was carried out to better understand the differing stability limits of PgNaN and PgNgN based OECTs. Upon increasing application of a reducing potential, the two main neutral absorption features (centered ~500 nm and ~900 nm) increasingly diminished, while new polaron absorption features emerged (with a maximum between 1000 and 1050 nm, 1100 and 1150 nm, and one with a maximum at wavelengths longer than

1300 nm, beyond the range of the detector), as shown in Figure 3a-b. At voltages close to the threshold voltage of each polymer device, the neutral absorptions were both present but reduced in intensity. The polaron absorption between 1000 and 1050 nm was heavily conflated with the neutral absorption at ~900 nm, and the lower energy charged absorption had yet to significantly emerge. Approaching the gate voltage limit of stable OECT operation (0.6 V and 0.4 V for PgNaN and PgNgN, respectively), the absorption spectra were dominated by strong polaron absorption above 1000 nm with residual neutral absorption still present. Near the voltage stability limit and beyond, an additional low energy absorption with a peak beyond the accessible range (>1300 nm) emerged.

Table 2. OECT performance of the polymers.

Polymer	$\mu_{sat,\ OECT}$ ($cm^2\ V^{-1}\ s^{-1}$)[c]	C* ($F\ cm^{-3}$)[d]	μ_{sat}×C* ($F\ cm^{-1}\ V^{-1}\ s^{-1}$)[e]	μC* ($F\ cm^{-1}\ V^{-1}\ s^{-1}$)[f]	$g_{m,\ max,\ norm.}$ ($S\ cm^{-1}$)[f]	on/off ratio
PgNaN	$(6.50 \pm 1.01) \times 10^{-3}$	100 ± 6	0.652 ± 0.107	0.662 ± 0.113	0.212	~10^4
PgNgN	$(1.89 \pm 0.23) \times 10^{-4}$	239 ± 97	0.046 ± 0.024	0.037 ± 0.016	0.007	~10^3
BBL[a]	7×10^{-4}	930	0.65	~0.6	0.3	~10^4
P90[b]	2.4×10^{-4}	200	0.048	~0.06	0.021	~10^4

[a] From reference.[16] [b] From reference.[5b] [c] Saturation mobility extracted from the slope of $I_d^{1/2}$ vs V_g. [d] Volumetric capacitance measured with electrochemical impedance spectroscopy. [e] The product of the saturation mobility and the volumetric capacitance. [f] Extracted from the slope of OECT transfer curves and normalized by channel thickness and aspect ratio.

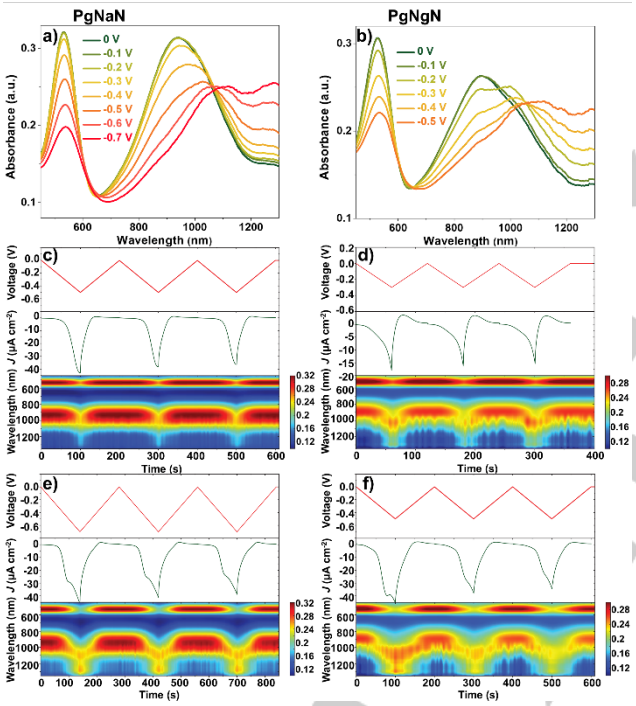

Figure 3. Spectroelectrochemistry: Potential dependent UV-Vis-NIR absorption spectra of (a) PgNaN and (b) PgNgN. Voltage profiles, current traces, and absorption color maps of (c) PgNaN and (d) PgNgN cycled within the window of voltage stability. Voltage profiles, current traces, and absorption color maps of (e) PgNaN and (f) PgNgN cycled beyond the window of voltage stability. Note the cumulative cycle by cycle changes in current trace and absorption color maps in panel (f), indicating film degradation.

While collecting absorbance spectra, films were cycled to potentials 50 mV below their apparent OECT stability limit (Figure 3c-d) and 50 mV beyond their apparent OECT stability limit (Figure 3e-f). To replicate OECT testing, these measurements were carried out in ambient conditions (i.e. exposed to ambient oxygen). The current traces show a large negative current indicative of potential side reactions that overshadow the polymer charging current, which is common with OECT materials in these potential ranges.[18] Below the apparent OECT stability limit, absorption color maps exhibited repeatable inducing of charged absorbing species for both polymers, as shown in Figure 3c-d. Beyond the apparent OECT stability limit, the low energy absorption of PgNgN decayed with each cycle, as shown in the color map in Figure 3f. Further, the PgNgN charging peak/shoulder in the current traces during negative potential sweeps was significantly diminished after each cycle. This seemed to indicate that charged species were not stable at these potentials and their presence irreversibly degraded the polymer such that these states were no longer electrochemically accessible upon further cycling. Conversely, PgNaN displayed largely reversible absorption spectra changes even when cycled beyond the apparent OECT stability limit, with current traces retaining the PgNaN charging shoulder each cycle. Thus it seems that though these electrochemical states are still accessible, charges in these states are much less mobile after cycling PgNaN beyond 0.6 V. This reversible charging of the PgNaN film at potentials where device degradation occurred (as assessed by OECT drain current decreases), indicates that the stability of PgNaN and PgNgN were limited by different processes.

Grazing incidence wide angle X-ray scattering (GIWAXS) was carried out to investigate the microstructure of the two polymer thin films and to establish a link between morphology and OECT performance. As shown in Figure 4a-b, both films displayed an isotropic ring of amorphous like scattering pattern centered around 1.5 $Å^{-1}$, along with rather isotropic lamellar scattering (100) indicating a broad distribution of crystallite orientations. The out-of-plane first order lamellar peak was conflated with a strong specular ridge, though second and third order (h00) peaks were identifiable. In-plane, the (100) peak was clearly resolved, though higher order peaks were not apparent. PgNaN showed increased scattering intensity from the π-stack in- and out-of-plane, while PgNgN π-stack scattering was predominately out-of-plane, as highlighted in the line cuts in Figure S16. This indicated a preferred face-on orientation of the crystallites in PgNgN, while PgNaN displayed a mix of edge-on and face-on oriented crystallites. The face-on orientation of the all glycol PgNgN was

similar to the previously reported all alkyl side chain analogue.[10c] Lamellar d-spacing, calculated from the in-plane (100) peak center, were 2 Å narrower for the mixed alkyl/glycol side chain PgNaN (28.3 Å), compared to the all glycol PgNgN (30.3 Å). PgNaN displayed an expanded π-stack d-spacing (3.76 Å) compared to PgNgN (3.65 Å) (listed in Table S1). While decreased π-stack d-spacing is at times correlated with improved charge transport (presumably due to improved molecular orbital overlap), in this case the polymer with the expanded π-stack (PgNaN) had the better charge transport. The mix of edge-on and face-on crystallites in PgNaN may be beneficial for three-dimensional charge transport which dominates in OECTs. Comparisons of similar conformationally locked polymers showed improved 2D transport (OFET) in predominantly face on textured films, and improved 3D transport (bulk molecular doped) in mixed face-on and edge-on textured films.[19] Additionally, peak width estimates of the coherence length of the π-stacking show that PgNaN π-stack ordering extended for 30-75% greater distances than that of PgNgN, which could be a contributing factor to improved charge transport PgNaN.

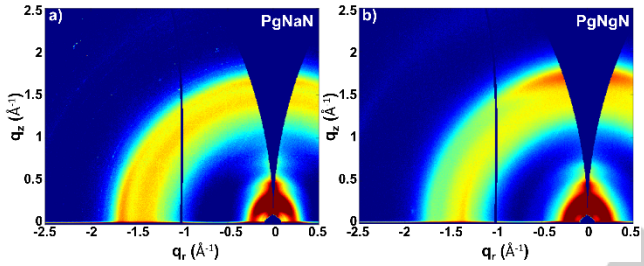

Figure 4. Two-dimensional grazing incidence wide angle scattering of (a) PgNaN and (b) PgNgN thin films.

In summary, we have developed two n-type conjugated polymers, PgNaN and PgNgN, bearing OEG side chains. Owing to their all electron-deficient polymer backbone, both polymers exhibit a deep-lying LUMO energy level lower than -4.0 eV, which is beneficial for electron transport. Arising from the aldol condensation polymerization process, the polymer backbone is fully conformationally locked, with no single linking bonds, thus promoting coplanarity and delocalization of molecular orbitals along the aryl lactam repeat units. These features contribute to the high OECT mobility of the polymers, which results in a maximum dimensionally normalized transconductance of 0.212 S cm^{-1} and the product μC* of 0.662 ± 0.113 F cm^{-1} V^{-1} s^{-1} for the PgNaN polymer.

Acknowledgements

The research reported in this publication was supported by funding from King Abdullah University of Science and Technology Office of Sponsored Research (OSR) under awards no. OSR-2018-CARF/CCF-3079, no. OSR-2015-CRG4-2572 and OSR-2019-CRG8-4086. We acknowledge EC FP7 Project SC2 (610115), EC H2020 (643791), and EPSRC Projects EP/G037515/1, EP/M005143/1, and EP/L016702/1. B.D.P., R.W., and J.R. gratefully acknowledge support from the National Science Foundation grant no. NSF DMR-1751308. Special thanks to Joseph Strzalka and Qingteng Zhang for beam line assistance. This research used resources of the Advanced Photon Source, a U.S. Department of Energy (DOE) Office of Science User Facility operated for the DOE Office of Science by Argonne National Laboratory under Contract No. DE-AC02-06CH11357. This work utilized Keck-II facility of Northwestern University's NUANCE Center and Northwestern University Micro/Nano Fabrication Facility (NUFAB), which are both partially supported by Soft and Hybrid Nanotechnology Experimental (SHyNE) Resource (NSF ECCS-1542205), the Materials Research Science and Engineering Center (NSF DMR-1720139), the State of Illinois, and Northwestern University. Additionally, the Keck-II facility is partially supported by the International Institute for Nanotechnology (IIN); the Keck Foundation; and the State of Illinois, through the IIN.

Keywords: rigid semiconducting polymer • n-type conjugated polymer• organic electrochemical transistors • oligo(ethylene glycol) side chain • metal-free aldol condensation

[1] a) M. Berggren, A. Richter-Dahlfors, *Adv. Mater.* **2007**, *19*, 3201-3213; b) R. A. Picca, K. Manoli, E. Macchia, L. Sarcina, C. Di Franco, N. Cioffi, D. Blasi, R. Österbacka, F. Torricelli, G. Scamarcio, L. Torsi, *Adv. Funct. Mater.* **2019**, *30*, 1904513; c) M. Ghittorelli, L. Lingstedt, P. Romele, N. I. Craciun, Z. M. Kovacs-Vajna, P. W. M. Blom, F. Torricelli, *Nat. Commun.* **2018**, *9*, 1441; d) M. Hamedi, R. Forchheimer, O. Inganas, *Nat. Mater.* **2007**, *6*, 357-362; e) M. Braendlein, A. M. Pappa, M. Ferro, A. Lopresti, C. Acquaviva, E. Mamessier, G. G. Malliaras, R. M. Owens, *Adv. Mater.* **2017**, *29*, 1605744; f) D. Ohayon, G. Nikiforidis, A. Savva, A. Giugni, S. Wustoni, T. Palanisamy, X. Chen, I. P. Maria, E. Di Fabrizio, P. Costa, I. McCulloch, S. Inal, *Nat. Mater.* **2020**, *19*, 456-463; g) N. Wang, A. Yang, Y. Fu, Y. Li, F. Yan, *Acc. Chem. Res.* **2019**, *52*, 277-287; h) L. Q. Flagg, C. G. Bischak, J. W. Onorato, R. B. Rashid, C. K. Luscombe, D. S. Ginger, *J. Am. Chem. Soc.* **2019**, *141*, 4345-4354.

[2] a) B. D. Paulsen, K. Tybrandt, E. Stavrinidou, J. Rivnay, *Nat. Mater.* **2020**, *19*, 13-26. b) E. Zeglio, O. Inganas, *Adv. Mater.* **2018**, *30*, 1800941; c) J. Rivnay, S. Inal, A. Salleo, R. M. Owens, M. Berggren, G. G. Malliaras, *Nat. Rev. Mater.* **2018**, *3*, 17086; d) M. Sessolo, J. Rivnay, E. Bandiello, G. G. Malliaras, H. J. Bolink, *Adv. Mater.* **2014**, *26*, 4803-4807; e) X. Wu, A. Surendran, J. Ko, O. Filonik, E. M. Herzig, P. Muller-Buschbaum, W. L. Leong, *Adv. Mater.* **2019**, *31*, 1805544.

[3] a) D. Khodagholy, J. Rivnay, M. Sessolo, M. Gurfinkel, P. Leleux, L. H. Jimison, E. Stavrinidou, T. Herve, S. Sanaur, R. M. Owens, G. G. Malliaras, *Nat. Commun.* **2013**, *4*, 2133; b) C. B. Nielsen, A. Giovannitti, D. T. Sbircea, E. Bandiello, M. R. Niazi, D. A. Hanifi, M. Sessolo, A. Amassian, G. G. Malliaras, J. Rivnay, I. McCulloch, *J. Am. Chem. Soc.* **2016**, *138*, 10252-10259.

[4] a) A. Facchetti, *Mater. Today* **2007**, *10*, 28-37; b) H. Sirringhaus, *Adv. Mater.* **2014**, *26*, 1319-1335; c) L. Lu, T. Zheng, Q. Wu, A. M. Schneider, D. Zhao, L. Yu, *Chem. Rev.* **2015**, *115*, 12666-12731; d) K. H. Hendriks, G. H. Heintges, V. S. Gevaerts, M. M. Wienk, R. A. Janssen, *Angew. Chem. Int. Ed.* **2013**, *52*, 8341-8344; e) A. F. Paterson, S. Singh, K. J. Fallon, T. Hodsden, Y. Han, B. C. Schroeder, H. Bronstein, M. Heeney, I. McCulloch, T. D. Anthopoulos, *Adv. Mater.* **2018**, *30*, 1801079; f) H. Bronstein, C. B. Nielsen, B. C. Schroeder, I. McCulloch, *Nat. Rev. Chem.* **2020**, *4*, 66-77.

[5] a) R. Giridharagopal, L. Q. Flagg, J. S. Harrison, M. E. Ziffer, J. Onorato, C. K. Luscombe, D. S. Ginger, *Nat. Mater.* **2017**, *16*, 737-742; b) A. Giovannitti, I. P. Maria, D. Hanifi, M. J. Donahue, D. Bryant, K. J. Barth, B. E. Makdah, A. Savva, D. Moia, M. Zetek, P. R. F. Barnes, O. G. Reid, S. Inal, G. Rumbles, G. G. Malliaras, J. Nelson, J. Rivnay, I. McCulloch, *Chem. Mater.* **2018**, *30*, 2945-2953;

c) B. X. Dong, C. Nowak, J. W. Onorato, J. Strzalka, F. A. Escobedo, C. K. Luscombe, P. F. Nealey, S. N. Patel, *Chem. Mater.* **2019**, *31*, 1418-1429.

[6] a) A. Giovannitti, D. T. Sbircea, S. Inal, C. B. Nielsen, E. Bandiello, D. A. Hanifi, M. Sessolo, G. G. Malliaras, I. McCulloch, J. Rivnay, *Proc. Natl. Acad. Sci. USA* **2016**, *113*, 12017-12022; b) L. R. Savagian, A. M. Osterholm, J. F. Ponder, Jr., K. J. Barth, J. Rivnay, J. R. Reynolds, *Adv. Mater.* **2018**, *30*, 1804647; c) P. K. Johansson, D. Jullesson, A. Elfwing, S. I. Liin, C. Musumeci, E. Zeglio, F. Elinder, N. Solin, O. Inganas, *Sci. Rep.* **2015**, *5*, 11242; d) P. Schmode, D. Ohayon, P. M. Reichstein, A. Savva, S. Inal, M. Thelakkat, *Chem. Mater.* **2019**, *31*, 5286-5295.

[7] a) H. D. Sun, J. Gerasimov, M. Berggren, S. Fabiano, *J. Mater. Chem. C* **2018**, *6*, 11778-11784; b) M. Moser, J. F. Ponder, A. Wadsworth, A. Giovannitti, I. McCulloch, *Adv. Funct. Mater.* **2018**, *29*, 1807033.

[8] a) J. T. E. Quinn, J. X. Zhu, X. Li, J. L. Wang, Y. N. Li, *J. Mater. Chem. C* **2017**, *5*, 8654-8681; b) J. Yang, Z. Y. Zhao, S. Wang, Y. L. Guo, Y. Q. Liu, *Chem* **2018**, *4*, 2748-2785; c) C. Yan, S. Barlow, Z. Wang, H. Yan, A. K. Y. Jen, S. R. Marder, X. Zhan, *Nat. Rev. Mater.* **2018**, *3*, 18003; d) M. Kim, S. U. Ryu, S. A. Park, K. Choi, T. Kim, D. Chung, T. Park, *Adv. Funct. Mater.* **2019**, *30*, 1904545.

[9] a) M. Hultell, S. Stafstrom, *Phys. Rev. B* **2007**, *75*, 104304; b) K. Zaugg, J. Velasco, K. A. Robins, D. C. Lee, *ACS Omega* **2019**, *4*, 5434-5441; c) Z. Ding, X. Long, C. Dou, J. Liu, L. Wang, *Chem. Sci.* **2016**, *7*, 6197-6202.

[10] a) K. Takimiya, I. Osaka, M. Nakano, *Chem. Mater.* **2013**, *26*, 587-593; b) Z. Wang, C. Kim, A. Facchetti, T. J. Marks, *J. Am. Chem. Soc.* **2007**, *129*, 13362-13363; c) A. Onwubiko, W. Yue, C. Jellett, M. Xiao, H. Y. Chen, M. K. Ravva, D. A. Hanifi, A. C. Knall, B. Purushothaman, M. Nikolka, J. C. Flores, A. Salleo, J. L. Bredas, H. Sirringhaus, P. Hayoz, I. McCulloch, *Nat. Commun.* **2018**, *9*, 416.

[11] a) A. Giovannitti, K. J. Thorley, C. B. Nielsen, J. Li, M. J. Donahue, G. G. Malliaras, J. Rivnay, I. McCulloch, *Adv. Funct. Mater.* **2018**, *28*, 1706325; b) Y. Wang, E. Zeglio, H. Liao, J. Xu, F. Liu, Z. Li, I. P. Maria, D. Mawad, A. Herland, I. McCulloch, W. Yue, *Chem. Mater.* **2019**, *31*, 9797-9806; c) A. Giovannitti, C. B. Nielsen, D. T. Sbircea, S. Inal, M. Donahue, M. R. Niazi, D. A. Hanifi, A. Amassian, G. G. Malliaras, J. Rivnay, I. McCulloch, *Nat. Commun.* **2016**, *7*, 13066.

[12] a) X. Chen, Z. Zhang, Z. Ding, J. Liu, L. Wang, *Angew. Chem. Int. Ed.* **2016**, *55*, 10376-10380; b) B. Meng, H. Song, X. Chen, Z. Xie, J. Liu, L. Wang, *Macromolecules* **2015**, *48*, 4357-4363; c) X. X. Chen, Z. J. Zhang, J. Liu, L. X. Wang, *Polym. Chem.* **2017**, *8*, 5496-5503.

[13] a) S. Torabi, F. Jahani, I. Van Severen, C. Kanimozhi, S. Patil, R. W. A. Havenith, R. C. Chiechi, L. Lutsen, D. J. M. Vanderzande, T. J. Cleij, J. C. Hummelen, L. J. A. Koster, *Adv. Funct. Mater.* **2015**, *25*, 150-157; b) M. Breselge, I. Van Severen, L. Lutsen, P. Adriaensens, J. Manca, D. Vanderzande, T. Cleij, *Thin Solid Films* **2006**, *511*, 328-332; c) S. Zhang, Z. J. Zhang, J. Liu, L. X. Wang, *Adv. Funct. Mater.* **2016**, *26*, 6107-6113.

[14] a) A. Savva, R. Hallani, C. Cendra, J. Surgailis, T. C. Hidalgo, S. Wustoni, R. Sheelamanthula, X. Chen, M. Kirkus, A. Giovannitti, A. Salleo, I. McCulloch, S. Inal, *Adv. Funct. Mater.* **2020**, *30*, 1907657; b) M. Moser, T. C. Hidalgo, J. Surgailis, J. Gladisch, S. Ghosh, R. Sheelamanthula, Q. Thiburce, A. Giovannitti, A. Salleo, N. Gasparini, A. Wadsworth, I. Zozoulenko, M. Berggren, E. Stavrinidou, S. Inal, I. McCulloch, *Adv. Mater.* **2020**, *32*, 2002748; c) M. Moser, L. R. Savagian, A. Savva, M. Matta, J. F. Ponder, T. C. Hidalgo, D. Ohayon, R. Hallani, M. Reisjalali, A. Troisi, A. Wadsworth, J. R. Reynolds, S. Inal, I. McCulloch, *Chem. Mater.* **2020**, *32*, 6618-6628.

[15] B. Scrosati in *Applications of Electroactive Polymers*, Eds.: G. Stienen, Springer, **1993**, pp. 1-23.

[16] H. Sun, M. Vagin, S. Wang, X. Crispin, R. Forchheimer, M. Berggren, S. Fabiano, *Adv. Mater.* **2018**, *30*, 1704916.

[17] a) V. Kaphle, S. Liu, A. Al-Shadeedi, C. M. Keum, B. Lussem, *Adv. Mater.* **2016**, *28*, 8766-8770; b) J. T. Friedlein, J. Rivnay, D. H. Dunlap, I. McCulloch, S. E. Shaheen, R. R. McLeod, G. G. Malliaras, *Appl. Phys. Lett.* **2017**, *111*, 023301; c) V. Kaphle, P. R. Paudel, D. Dahal, R. K. Radha Krishnan, B. Lussem, *Nat. Commun.* **2020**, *11*, 2515.

[18] A. Savva, S. Wustoni, S. Inal, *J. Mater. Chem. C* **2018**, *6*, 12023-12030.

[19] M. Alsufyani, R. K. Hallani, S. Wang, M. Xiao, X. Ji, B. D. Paulsen, K. Xu, H. Bristow, H. Chen, X. Chen, H. Sirringhaus, J. Rivnay, S. Fabiano, I. McCulloch, *J. Mater. Chem. C* **2020**, DOI: 10.1039/D0TC03347B.

X. Chen,* A. Marks, B. D. Paulsen, R. Wu, R. B. Rashid, H. Chen, M. Alsufyani, J. Rivnay, and I. McCulloch*

Page No. – Page No.

N-type Rigid Semiconducting Polymers Bearing Oligo(Ethylene Glycol) Side Chains for High Performance Organic Electrochemical Transistors

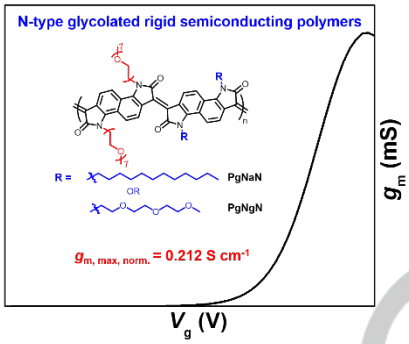

Two new n-type semiconducting polymers, PgNaN and PgNgN, bearing oligo(ethylene glycol) (OEG) side chain are developed with a fully conformationally locked backbone and deep-lying LUMO energy level. As a result, the polymer of PgNaN exhibits a good performance on OECT device with a maximum dimensionally normalized transconductance of 0.212 S cm^{-1} and the product μC* of 0.662 ± 0.113 F cm^{-1} V^{-1} s^{-1}.